

# Acoustic Vector-Sensor Processing in the Presence of a Reflecting Boundary

Malcolm Hawkes, *Member, IEEE*, and Arye Nehorai, *Fellow, IEEE*

**Abstract**—We consider the passive direction-of-arrival (DOA) estimation problem using arrays of acoustic vector sensors located in a fluid at or near a reflecting boundary. We formulate a general measurement model applicable to any planar surface, derive an expression for the Cramér–Rao bound (CRB) on the azimuth and elevation of a single source, and obtain a bound on the mean-square angular error (MSAE). We then examine two applications of great practical interest: hull-mounted and seabed arrays. For the former, we use three models for the hull: an ideal rigid surface for high frequency, an ideal pressure-release surface for low frequency, and a more complex, realistic layered model. For the seabed scenario, we model the ocean floor as an absorptive liquid layer. For each application, we use the CRB, MSAE bound, and beampatterns to quantify the advantages of using velocity and/or vector sensors instead of pressure sensors. For the hull-mounted application, we show that normal component velocity sensors overcome the well-known, low-frequency problem of small pressure signals without the need for an undesirable “stand-off” distance. For the seabed scenario, we also derive a fast wideband estimator of the source location using a single vector sensor.

## I. INTRODUCTION

**T**RADITIONALLY, acoustic fields in fluids have been measured using pressure sensors. Recently, the idea of using *vector* sensors that measure both pressure and velocity was introduced to the signal processing community in [1] and [2] and used to solve the passive direction-of-arrival (DOA) estimation problem [1]–[9]. Much work is currently being done on the development of velocity sensors [5], and complete vector sensors have already been constructed and tested at sea [10], [11].

Previous work, e.g., [2]–[9], has only considered arrays of acoustic vector sensors in free space; however, there are numerous important applications in which it is required to estimate the DOA of an acoustic wave traveling in a fluid in the presence of reflecting boundaries. Examples include hull-mounted sonar, in which sensors are located on a vessel’s hull, providing a great operational advantage over towed arrays; bottom-tethered sonar, where arrays of sensor are moored to the ocean floor for long-term surveillance; and floating sonar arrays, i.e., an array of sensors, each of which is located just below the surface tethered to a buoy. There are also

aero-acoustic applications, for example, battlefield surveillance [12], [13], where reflections from the ground must be taken into account, and microphone arrays for teleconferencing, which must operate in an environment with many reflecting boundaries.

In this paper (see also [14] and [15]), we derive a general model for the measurements made by a planar array of vector sensors, each of which measures pressure and all components of particle velocity at a single point, when it is located at or near a planar interface with an arbitrary solid or fluid half space. We obtain an expression for the Cramér–Rao bound (CRB) on the azimuth and elevation of a single source and use it to calculate a bound on the mean-square angular error (MSAE) for a large class of estimators (see [16] and [17]). Using these measures of optimal performance, we study the advantages of using arrays of velocity and vector sensors, as opposed to traditional pressure-sensor arrays, for DOA estimation in a variety of practical applications.

A problem of particular practical significance arises in hull-mounted sonar. At low frequencies, a vessel’s hull becomes acoustically flexible or compliant with the result that the pressure signal on or near the surface is very low, leading to poor performance [18], [19]. One solution is to mount pressure sensors such that they “stand off” from the surface some distance. A large stand-off distance is highly undesirable because it gives the vessel a large profile, thereby increasing drag and detectability. However, it can be avoided by using normal-component velocity sensors mounted on the surface. Although this solution allows flush-mounted sensors, it cannot, as we show, outperform an array of pressure sensors at a large enough stand-off distance. Using an ideal pressure-release model for the hull, we compare the performance of a flush-mounted velocity sensor array with a stand-off array of pressure sensors and determine the minimum stand-off distance at which the arrays have comparable performance. More generally, employing a realistic four-layered model of the hull, we show that an array of complete four-component vector sensors can, when mounted at a much-reduced distance from the hull, equal or improve on the performance of a pressure-sensor array, no matter how large its stand-off distance. We also examine the high-frequency case, when the surface is acoustically hard, by using an idealized rigid surface. In this situation, we quantify the advantage of adding in-plane velocity components and, using the beampattern, show that their addition resolves ambiguities caused by spatial undersampling.

We then consider the problem of passive sonar arrays mounted on the ocean floor by modeling the seabed as an absorptive liquid layer. We compare full four-component

Manuscript received December 2, 1999; revised July 6, 2000. This work was supported by the Air Force Office of Scientific Research under Grants F49620-97-1-0481 and F49620-99-1-0067, the National Science Foundation under Grant MIP-9615590, and the Office of Naval Research under Grant N00014-98-1-0542. The associate editor coordinating the review of this paper and approving it for publication was Prof. Jian Li.

The authors are with the Department of Electrical Engineering and Computer Science, University of Illinois, Chicago, IL 60607 USA (e-mail: nehorai@eecs.uic.edu; hawkes@eecs.uic.edu).

Publisher Item Identifier S 1053-587X(00)09297-7.

vector-sensor arrays with pressure-sensor arrays, mounted both directly on the bottom and slightly above it, as in a moored deployment, for example. The vector-sensor array's performance is shown to be markedly superior and almost isotropic. For this scenario, we also derive and analyze a fast wideband estimator for use with a single vector sensor.

In Section II, we derive the measurement model for an array located near a reflecting boundary. Then, in Section III, we derive general optimal performance results for this model. Section IV discusses the hull-mounted sonar problem and Section V the seabed array. Section VI concludes the paper.

## II. MEASUREMENT MODEL

Consider a planewave traveling in a quiescent, isotropic, homogeneous, infinite fluid half space, bounded by an infinite planar interface. When the planewave hits the boundary, it produces a reflected wave traveling back into the fluid and one or more transmitted waves that continue to propagate past the interface. If the incident planewave is monochromatic, the reflected planewave is also monochromatic but exhibits a change of amplitude and phase. At position  $\mathbf{r}$  and time  $t$ , the (complex) pressure field in the fluid, due to the incident and reflected waves, is given by

$$\begin{aligned} p_i(\mathbf{r}, t) &= \tilde{p} \exp i(\omega t - \mathbf{k}_i^T \mathbf{r}) \\ p_r(\mathbf{r}, t) &= \tilde{p} \mathcal{R} \exp i(\omega t - \mathbf{k}_r^T \mathbf{r}) \end{aligned} \quad (1)$$

respectively, where  $\tilde{p}$  is the complex amplitude of the incident wave,  $\mathbf{k}_i$  and  $\mathbf{k}_r$  are the incident and reflected wavenumber vectors,  $\omega$  is the angular frequency, and  $\mathcal{R}$  is the (complex) reflection coefficient, which specifies the attenuation and phase change of the reflected wave. Note that the wavenumber vector points in the direction of propagation of the wave and has modulus  $\omega/c$ , where  $c$  is the speed of sound in the fluid. Physical considerations require that the normal particle velocities on either side of the boundary are equal, which implies that the incident and reflected waves travel along the boundary with identical velocities [20]. This means that the reflected wavenumber vector  $\mathbf{k}_r$  is obtained by reflecting the incident wavenumber vector in the plane of the interface.

The half space that reflects the wave may be solid or fluid, homogeneous or layered, or even have continuously changing properties. In fact, in order for (1) to hold, the essential characteristic of the second half-space is that its material properties are constant on any plane parallel to the interface with the fluid. Note that this implies that the interface is smooth with respect to the wavelength of the incident wave so that the reflection is specular.

For both the incident and reflected waves, pressure is related to particle velocity  $\mathbf{v}$  by Euler's equation, which for planewaves becomes (e.g., [21])

$$\mathbf{v}(\mathbf{r}, t) = \frac{p(\mathbf{r}, t)}{\omega \rho_0} \mathbf{k} \quad (2)$$

where  $\rho_0$  is the ambient fluid density. The total field in the fluid is given by the superposition of the incident and reflected waves that interfere to form a standing wave pattern. We choose

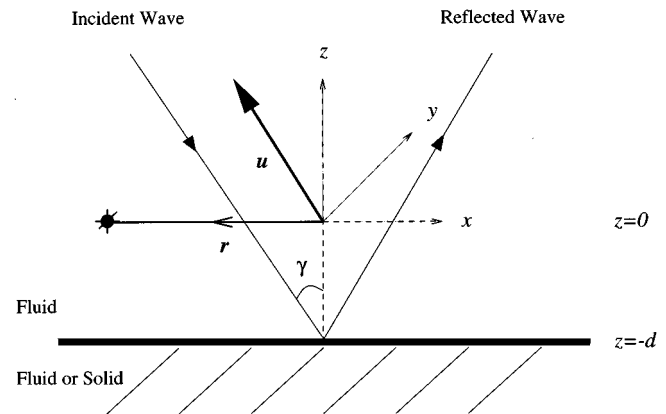


Fig. 1. Schematic illustration of reflection of incident wave at boundary; the incident and reflected waves interfere to form a standing wave pattern. A sensor assumed to lie in the  $z = 0$  plane and its position vector  $\mathbf{r}$ , along with the incidence angle  $\gamma$  and bearing vector  $\mathbf{u}$  of the source, are also shown.

our coordinate system such that the interface coincides with the plane  $z = -d$  with the  $z$  axis pointing into the fluid (see Fig. 1). The reflected wavenumber vector  $\mathbf{k}_r$  is then obtained from  $\mathbf{k}_i$  by negating the  $z$ -component. Suppressing the dependence on time, the total pressure and velocity fields in the fluid at  $\mathbf{r} = [x, y, 0]^T$  are

$$p(\mathbf{r}) = \tilde{p} e^{-i(k_x x + k_y y)} (1 + \mathcal{R} e^{i2k_z d}) \quad (3)$$

$$\mathbf{v}(\mathbf{r}) = \tilde{p} \frac{e^{-i(k_x x + k_y y)}}{\omega \rho_0} \begin{bmatrix} k_x (1 + \mathcal{R} e^{i2k_z d}) \\ k_y (1 + \mathcal{R} e^{i2k_z d}) \\ k_z (1 - \mathcal{R} e^{i2k_z d}) \end{bmatrix} \quad (4)$$

where  $k_x$ ,  $k_y$ , and  $k_z$  are the components of the incident wavenumber vector  $\mathbf{k}_i$ .

### A. Reflection Coefficient

The reflection coefficient  $\mathcal{R}$  expresses the attenuation and phase change of the reflected planewave. It is highly dependent on the nature of both half spaces and is generally a function of both frequency and incidence angle. It may be expressed as a function of the boundary's input impedance, which is defined as the ratio of the (complex) pressure to the (complex) normal component of particle velocity at the surface [21]

$$Z_{\text{in}} = -(p(\mathbf{r})/v_n(\mathbf{r}))|_{z=-d} \quad (5)$$

where  $v_n$  is the component of  $\mathbf{v}$  normal to the boundary. As long as the surface is flat, of uniform composition over any plane parallel to the boundary, and of large extent,  $Z_{\text{in}}$  is the same at all points on the surface. As may be derived from (3) and (4), the reflection coefficient is related to  $Z_{\text{in}}$  by

$$\mathcal{R} = \frac{Z_{\text{in}} - Z}{Z_{\text{in}} + Z} \quad (6)$$

where  $Z = \rho_0 c / \cos \gamma$  is the impedance of the incident wave, and  $\gamma$  is the incidence angle. Equation (6) also appears in the theory of transmission and propagation of electromagnetic waves [22].

In general, for a fixed frequency, the dependence of  $Z_{\text{in}}$  on  $\gamma$  may be quite complex. Fortunately, there are several ideal situ-

ations of practical interest that simplify the situation considerably.

- i) If  $|Z_{\text{in}}| \rightarrow \infty$ , then  $\mathcal{R} = 1$  for all incidence angles. Such a surface is called a *rigid* boundary and occurs at high frequency in hull-mounted sonar and in room acoustics, for example.
- ii) If  $|Z_{\text{in}}| \rightarrow 0$ , then  $\mathcal{R} = -1$ , which is again independent of incidence angle. This surface is called a *pressure-release* boundary and (to a first approximation) describes the reflective properties of a vessel's hull at low frequency [18]. It is also a good approximation for underwater sound reflected from the interface with the air [21, p. 135] and is relevant to a floating or towed array scenario.
- iii) If  $Z_{\text{in}}$  is independent of incidence angle,  $\mathcal{R}$  is a fairly simple function of  $\gamma$ . Such a surface is called *locally reacting* and occurs with porous sound-absorbing materials [13, p. 13] and grass-covered ground surfaces [23].

Somewhat more complex analytic expressions for  $\mathcal{R}$  in terms of incidence angle are available when the reflecting half-space is another fluid or a homogeneous or stratified solid [20]. We will use them for modeling reflection at the ocean floor and as a second approximation to a vessel's hull.

### B. Array Measurements

Consider an array of sensors mounted on or near the interface such that each measures the acoustic pressure and/or acoustic particle velocity *in the fluid* at its location. We will allow for their distance from the interface to be zero, i.e., the sensors measure the fluid velocity at the interface. To do so, we are making the standard approximations [21] that the effects of fluid viscosity and thermal conduction are negligible and that slip is possible at the boundary, i.e., the tangential particle velocities on either side of the interface may be discontinuous. In practice, of course, sensors mounted on the interface should protrude just enough to avoid any boundary layer. To develop the model, we suppose that the array consists of vector sensors, each of which is formed from a co-located pressure sensor and triad of orthogonal velocity sensors. Arrays of pressure sensors, pressure plus in-plane velocity sensors, and normal-component velocity sensors, all of which we will consider, are just special cases of this model.

Denote the azimuth and elevation of the far-field source corresponding to the incident wave by  $\phi$  and  $\psi$ , respectively. The incident wavenumber vector is then

$$\mathbf{k}_i = -\frac{\omega}{c} \begin{bmatrix} \cos \phi \cos \psi \\ \sin \phi \cos \psi \\ \sin \psi \end{bmatrix} = -\frac{\omega}{c} \mathbf{u} \quad (7)$$

where  $\mathbf{u}$  is the unit vector pointing toward the source, i.e., the bearing. Suppose a vector sensor is located in the  $z = 0$  plane with  $x, y$  coordinates  $\mathbf{r} = [r_x, r_y]^T$  (the boundary lies in the  $z = -d$  plane) and oriented such that its velocity sensors measure the velocity components parallel to the coordinate axes. This may be achieved by rotation of the data as long as the orientation of the sensor is known. Then, using (3) and (4), its noise-free

output would be a four-element vector of complex sinusoids with complex amplitudes

$$\begin{bmatrix} y_p \\ \mathbf{y}_v \end{bmatrix} = \tilde{p} e^{i2\pi \cos \psi \mathbf{r}^T \tilde{\mathbf{u}}} \cdot \begin{bmatrix} (1 + \mathcal{R}(\psi) e^{-i\vartheta}) \\ (1 + \mathcal{R}(\psi) e^{-i\vartheta}) \cos \phi \cos \psi \\ (1 + \mathcal{R}(\psi) e^{-i\vartheta}) \sin \phi \cos \psi \\ (1 - \mathcal{R}(\psi) e^{-i\vartheta}) \sin \psi \end{bmatrix} \quad (8)$$

where  $\tilde{\mathbf{u}} = [\cos \phi, \sin \phi]^T$ ,  $\vartheta \triangleq 4\pi d \sin \psi$ , the velocity measurements are normalized by  $-\rho_0 c$ , and all lengths are in units of wavelengths. Of course,  $y_p$  is the omnidirectional pressure sensor output, and  $\mathbf{y}_v$  is the  $3 \times 1$  output of the velocity sensor triad. By our choice of coordinate system, the incidence angle  $\gamma$  (see Fig. 1) is just  $\pi/2 - \psi$ ; therefore, for a given frequency,  $\mathcal{R}$  is a function of  $\psi$  but not  $\phi$ . We have expressed this dependence explicitly above.

The above model has been developed for monochromatic signals, but it can simply be extended to account for signals of finite bandwidth, i.e.,  $\tilde{p}$  varying with time. In that case, (8) gives the complex envelope (phasor representation) of the output of each sensor. The signal  $\tilde{p}(t)$  must be such that, for any given angle of incidence, the reflection coefficient is approximately constant over the bandwidth. Furthermore, reflections coming from strata within the reflecting half-space must die away in a much shorter time than the reciprocal of the bandwidth, which must also be much longer than the round trip travel time from the sensor to the boundary and back. The units of  $\mathbf{r}$  are  $d$  must then be in wavelengths corresponding to the center frequency, i.e., the frequency used for demodulation to obtain the baseband phasor representation.

Now, suppose we have an array consisting of  $m$  vector sensors located on or near the boundary in the plane  $z = 0$  and with  $x, y$  coordinates given by  $\mathbf{r}_1, \dots, \mathbf{r}_m$ . Again, we assume that the orientations of all sensors are known and that the data from each sensor has been rotated to align it with the coordinate axes. We must also make a narrowband assumption that the reciprocal of the bandwidth is much smaller than time taken for the incident wave *and* its reflection to propagate across the array. This is slightly more restrictive than the usual free-space narrowband assumption; for example, it could be violated by an array that is very far from the boundary, even though the array itself is very compact. This restriction must be satisfied in addition to the aforementioned bandwidth limitations. Which of these considerations actually limits the bandwidth in practice will depend on the scenario. Stacking the four-element vector outputs of each vector sensor into a  $4m$ -element vector gives the measurement model

$$\mathbf{y}(t) = \mathbf{a}(\boldsymbol{\theta}) \tilde{p}(t) + \mathbf{e}(t) \quad (9)$$

for  $t = 1, 2, \dots$ , where  $\boldsymbol{\theta} = [\phi, \psi]^T$  is the unknown DOA, and  $\mathbf{e}(t)$  is noise. By ensuring that all sensors lie in the same plane, we can express the steering vector  $\mathbf{a}(\boldsymbol{\theta})$  as the Kronecker product of the usual steering vector for a pressure-sensor array

in free space and a vector that incorporates the directional sensitivity of each component and the effect of the boundary. From (8), it follows that

$$\mathbf{a}(\boldsymbol{\theta}) = \mathbf{a}_p(\boldsymbol{\theta}) \otimes \mathbf{h}(\boldsymbol{\theta}) \quad (10)$$

where

$$\mathbf{a}_p(\boldsymbol{\theta}) = [e^{i2\pi \cos \psi \mathbf{r}_1^T \hat{\mathbf{u}}}, \dots, e^{i2\pi \cos \psi \mathbf{r}_m^T \hat{\mathbf{u}}}]^T \quad (11)$$

$$\mathbf{h}(\boldsymbol{\theta}) = \begin{bmatrix} (1 + \mathcal{R}(\psi)e^{-i\vartheta}) \\ (1 + \mathcal{R}(\psi)e^{-i\vartheta}) \\ (1 + \mathcal{R}(\psi)e^{-i\vartheta}) \\ (1 - \mathcal{R}(\psi)e^{-i\vartheta}) \end{bmatrix} \odot \begin{bmatrix} 1 \\ \mathbf{u} \end{bmatrix} \quad (12)$$

where  $\odot$  indicates the element-wise product.

The vector  $\mathbf{a}_p(\boldsymbol{\theta})$  is the steering vector of a free-space pressure sensor array and depends only on the  $x, y$  coordinates of the sensors' locations and not in any way on the closeness or nature of the boundary. It is mainly affected by the relationship between the azimuth of the incoming wave and the sensor locations; the effect of the elevation is identical for each term and is not complex. This vector effectively encodes the phase delay information resulting from the propagation delays between physically separated sensors. On the other hand,  $\mathbf{h}(\boldsymbol{\theta})$  depends only on the distance and nature of the boundary and not at all on the relative locations of the sensors. It is strongly affected by how the reflective properties of the boundary vary with elevation (incidence angle) but also encodes the velocity field information in the relative magnitudes of its components. Note that the assumption that all sensors lie in the plane is not inherently necessary; however, it does allow the steering vector to be expressed as a Kronecker product (10). This, in turn, will simplify many expressions in the subsequent analysis and allow us to gain a greater insight into the problem.

1) *Statistical Assumptions:* We assume that both  $\tilde{p}(t)$  and  $\mathbf{e}(t)$  are independent identically distributed (i.i.d.) complex circular Gaussian processes with zero-mean and that  $\tilde{p}(t)$  and  $\mathbf{e}(\tau)$  are independent for all  $t$  and  $\tau$ . These processes are completely characterized by their covariances

$$\mathbb{E}\{\tilde{p}(t)\tilde{p}^H(\tau)\} = \sigma_s^2 \delta_{t,\tau} \quad (13)$$

$$\mathbb{E}\{\mathbf{e}(t)\mathbf{e}^H(\tau)\} = \sigma^2 I_{4m} \delta_{t,\tau} \quad (14)$$

where the superscript  $H$  represents conjugate transposition,  $\sigma_s^2$  and  $\sigma^2$  are the signal and noise powers, respectively,  $I_{4m}$  is the  $4m$ th-order identity matrix, and  $\delta_{t,\tau}$  is the Kronecker delta function. There are four real unknowns: the two element DOA vector of interest  $\boldsymbol{\theta}$  and the signal and noise powers  $\sigma_s^2$  and  $\sigma^2$ , which are nuisance parameters. The assumed structure of the noise covariance is consistent with electronic sensor noise. Note that we have assumed the same noise power at pressure and velocity sensors for simplicity of exposition; however, incorporation of different noise powers for the different types of sensor is quite straightforward [1]–[3].

When ambient noise is the dominant noise source, noise powers at the different types of sensor will generally differ. For example, in spatially isotropic noise in free space, the noise power at each velocity sensor is one third of that at the pressure sensor, and it is uncorrelated between co-located sensors [24]. The lower velocity sensor noise power would mean that adding

velocity components provides even greater improvement than the results here indicate. When there is water flow past the sensors, which is the case if the vessel is moving in hull-mounted sonar, the different sensor types are also differently affected. For example, in one experiment, it was shown that if the flow was fast enough to become turbulent on the surface of the sensor packaging, then velocity sensors were more adversely affected than pressure sensors [25]. However, [26] showed that encasing the sensors in elastomer, which was not done in [25], can significantly reduce flow noise.

### III. OPTIMUM PERFORMANCE

The Cramér-Rao bound (CRB) is a lower bound on the variance of all unbiased estimators of a set of parameters and is achieved asymptotically by the maximum likelihood estimator under mild regularity conditions [27]. Using the results of [2], we derive an expression for the CRB on azimuth and elevation when there is a single source.

*Theorem III.1:* For the measurement model in Section II, with an arbitrary differentiable  $\mathbf{h}$ , and coordinate frame chosen such that the centroid of the planar array is at the origin, the CRB on the directional parameters is given by

$$\text{CRB}(\boldsymbol{\theta}) = \frac{1}{2Nm\rho|\mathbf{h}|^2} \left(1 + \frac{1}{m\rho|\mathbf{h}|^2}\right) (J + K)^{-1} \quad (15)$$

where  $\rho = \sigma_s^2/\sigma^2$  is the signal to noise ratio (SNR), and  $N$  is the number of snapshots. The matrices  $J$  and  $K$  are symmetric with the former given by

$$J = \frac{4\pi^2}{m} \begin{bmatrix} \cos^2 \psi S_{\phi\phi} & \sin \psi \cos \psi S_{\phi\psi} \\ \sin \psi \cos \psi S_{\phi\psi} & \sin^2 \psi S_{\psi\psi} \end{bmatrix} \quad (16)$$

where

$$\begin{aligned} S_{\phi\phi} &= \sum_{j=1}^m (\mathbf{r}_j^T \mathbf{v}_\phi)^2 \\ S_{\psi\psi} &= \sum_{j=1}^m (\mathbf{r}_j^T \mathbf{v}_\psi)^2 \\ S_{\phi\psi} &= \sum_{j=1}^m (\mathbf{r}_j^T \mathbf{v}_\phi)(\mathbf{r}_j^T \mathbf{v}_\psi) \end{aligned} \quad (17)$$

$\mathbf{v}_\phi = [-\sin \phi, \cos \phi]^T$  and  $\mathbf{v}_\psi = -[\cos \phi, \sin \phi]^T$ . The entries of  $K$  are

$$\begin{aligned} K_{11} &= \frac{1}{|\mathbf{h}|^2} \left( \left| \frac{\partial \mathbf{h}}{\partial \phi} \right|^2 - \frac{1}{|\mathbf{h}|^2} \left| \frac{\partial \mathbf{h}^H}{\partial \phi} \mathbf{h} \right|^2 \right) \\ K_{22} &= \frac{1}{|\mathbf{h}|^2} \left( \left| \frac{\partial \mathbf{h}}{\partial \psi} \right|^2 - \frac{1}{|\mathbf{h}|^2} \left| \frac{\partial \mathbf{h}^H}{\partial \psi} \mathbf{h} \right|^2 \right) \\ K_{12} = K_{21} &= \frac{1}{|\mathbf{h}|^2} \text{Re} \left\{ \frac{\partial \mathbf{h}^H}{\partial \phi} \frac{\partial \mathbf{h}}{\partial \psi} - \frac{1}{|\mathbf{h}|^2} \frac{\partial \mathbf{h}^H}{\partial \phi} \mathbf{h} \mathbf{h}^H \frac{\partial \mathbf{h}}{\partial \psi} \right\}. \end{aligned} \quad (18)$$

This result is the same whether  $\sigma^2$  is known or unknown. The CRB's for arrays consisting of pressure plus in-plane velocity

sensors, normal velocity sensors only, etc., are obtained by substituting the appropriate  $\mathbf{h}$  into (15) and (18).

*Proof:* Our model is a member of the class of vector-sensor models in [2, Th. 3.1], which presented a general expression for the CRB on the direction parameters for members of this class. The derivation is a generalization of that presented in [4] and is given in [28].

Observe that the matrix  $J$  depends only on the location of the sensors and not the nature of the sensors or the boundary—the vector  $\mathbf{h}$  describing the response of each individual sensor is not involved. It does so through the terms in (17), which are the sums of squares and products of projections of the sensors position vectors onto directions parallel  $\mathbf{v}_\phi$  and perpendicular  $\mathbf{v}_\psi$  to the projection of the bearing vector  $\mathbf{u}$  onto the  $x, y$  plane. Therefore, they essentially describe the squared array aperture “seen” by the source in these directions (see [4] for a fuller discussion of this concept for the free-space scenario). Conversely,  $K$  does not depend on the array geometry at all, but it incorporates both the directional sensitivity of the velocity sensors and the effect of the boundary through the reflection coefficient. We can therefore think of  $J$  as representing that part of the Fisher information that is due to the physical aperture, whereas  $K$  represents that information resulting from the directional sensitivity of the velocity sensors and the presence of the boundary. This separation of the Fisher information into the sum of a location-dependent but sensor-independent term and a sensor/boundary-dependent but location-independent term is analogous to, and a direct result of, splitting of the steering vector into the Kronecker product (10) of a phase delay term  $\mathbf{a}_P$  and a “within sensor” term  $\mathbf{h}$ .

For our particular  $\mathbf{h}$ , we can simplify (18) somewhat. If only one type of component is used in the array,  $\mathbf{h}$  contains only one element, and it follows that  $K = 0$ . When there is more than one component at each location, as long as both, or neither, of the in-plane velocity components are present

$$\frac{\partial \mathbf{h}^H}{\partial \phi} \mathbf{h} = \frac{\partial \mathbf{h}^H}{\partial \phi} \frac{\partial \mathbf{h}}{\partial \psi} = 0 \quad (19)$$

and all other terms in (18),  $|\mathbf{h}|^2$ , etc., are independent of  $\phi$  [28]. Thus,  $K$  becomes diagonal with

$$K_{11} = \frac{1}{|\mathbf{h}|^2} \left| \frac{\partial \mathbf{h}}{\partial \phi} \right|^2 \quad (20)$$

$$K_{22} = \frac{1}{|\mathbf{h}|^2} \left( \left| \frac{\partial \mathbf{h}}{\partial \psi} \right|^2 - \frac{1}{|\mathbf{h}|^2} \left| \frac{\partial \mathbf{h}^H}{\partial \psi} \mathbf{h} \right|^2 \right) \quad (21)$$

and depends only on the elevation and the proximity and reflective properties of the boundary.

In [16] (see also [17]), a framework is presented for the analysis of errors in estimating vectors and vector systems. The mean-square angular error (MSAE) is proposed as a useful overall error measure for the DOA estimation problem, and a bound is derived on the MSAE (normalized by the number of time samples,  $N$  say) that holds asymptotically for a large class of estimators. It is given by

$$\text{MSAE}_B(\boldsymbol{\theta}) = N \{ \cos^2 \psi \cdot \text{CRB}(\phi) + \text{CRB}(\psi) \} \quad (22)$$

which does not depend on  $N$  since the CRB is proportional to  $1/N$  for i.i.d. snapshots. We will examine performance in terms of this measure as well as the CRB for the various scenarios that we study.

We will simplify our expression further by choosing the constraints

$$\begin{aligned} \sum_{j=1}^m r_{jx} r_{jy} &= 0 \\ \sum_{j=1}^m r_{jx}^2 &= \sum_{j=1}^m r_{jy}^2 \end{aligned} \quad (23)$$

on the array geometry. These constraints, which essentially require the array to be symmetrical about the  $x$  and  $y$  axes, ensure that the off-diagonal entry of  $J$  is zero, as can be seen by evaluating  $S_{\phi\psi}$  in (17). In [4], this was argued to be a strong criterion for array design as it tends to minimize the CRB for a given physical array aperture; it also means that knowledge of one of the arrival angles does not affect the ability to optimally estimate the other. With these constraints

$$J = \frac{4\pi^2}{m} \sum_{j=1}^m r_{jx}^2 \begin{bmatrix} \cos^2 \psi & 0 \\ 0 & \sin^2 \psi \end{bmatrix} \quad (24)$$

and therefore, the CRB and, hence,  $\text{MSAE}_B$ , become completely independent of the azimuth  $\phi$ , thereby simplifying the interpretation of results.

#### IV. HULL-MOUNTED SCENARIO

In this section, we examine the hull-mounted sonar problem. In Section IV-A, we deal with the high-frequency case in which the hull behaves like a rigid surface. In Section IV-B, we then examine the low-frequency case in which the hull approximates a pressure-release surface. Finally, in Section IV-C, we consider a more complex layered model for the hull that is appropriate over a range of frequencies. Note that although a hull-mounted array will typically be located on the flank of a vessel, i.e., in a vertical plane, we still define our coordinate system such that the array lies in the  $x, y$ -plane and use the terms azimuth and elevation as defined by our coordinate system, rather than an earth referenced system.

##### A. Rigid Boundary

The rigid boundary condition occurs whenever the reflecting surface is not acoustically pliable, i.e., it does not move when an acoustic wave hits it, and is a good approximation to a vessel’s hull at high frequency. It is also the case in reflection from walls and other hard surfaces in room acoustics. Mathematically, the condition is expressed by  $\mathcal{R} = 1$  for all incidence angles. Setting  $d = 0$  and  $\mathcal{R} = 1$  in (3) and (4), we see that the normal velocity component is zero at such a boundary but that the pressure and in-plane velocity components are double their values in free space. In practice, arrays of pressure sensors flush mounted on the hull are used; therefore, it is of interest to consider whether the addition of in-plane velocity sensors offers a significant advantage.

As a result of the pressure doubling, a pressure-sensor array mounted on a rigid surface is equivalent to a pressure-sensor array in free space with an SNR four times as large, assuming

all noise is nonacoustic (clearly, the pressure of ambient noise will also be doubled). The CRB is given by (15) with  $|\mathbf{h}|^2 = 1$ ,  $\rho = 4\sigma_s^2/\sigma^2$ , and  $K = 0$ . Of course, this is the same as the expression for a pressure-sensor array in free space [3], except that we have an effective SNR of  $4\sigma_s^2/\sigma^2$  instead of  $\sigma_s^2/\sigma^2$  at each sensor—an increase of 6 dB.

For an array of sensors flush mounted on the surface, each of which measures the pressure and both in-plane velocity components, it follows from (12) that  $\mathbf{h} = [1, \cos \phi \cos \psi, \sin \phi \cos \psi]^T$ . Thus, the CRB is given by (15) with the effective SNR  $\rho|\mathbf{h}|^2 = 4\sigma_s^2(1 + \cos^2 \psi)/\sigma^2$ , and

$$K = \begin{bmatrix} \cos^2 \psi / (1 + \cos^2 \psi) & 0 \\ 0 & \sin^2 \psi / (1 + \cos^2 \psi)^2 \end{bmatrix}. \quad (25)$$

Therefore, the addition of in-plane velocity sensors increases the effective SNR by  $(1 + \cos^2 \psi)$  because of the greater number of measurements, and results in the extra additive term  $K$ , due to the directional sensitivity of the velocity sensors. Both these factors act to reduce the CRB. The effective SNR increase is largest (around 3 dB) near grazing incidence and becomes negligible near normal incidence. This becomes intuitive when we consider that the signal measured at the velocity sensors is greatest when the wave is parallel to the surface and zero when it is normal. Unlike the free-space case [3], the directional matrix  $K$  strongly depends on the bearing  $\mathbf{u}$ . This is a result of the dependence of the velocity-vector SNR (the SNR of the sum of the outputs from the velocity sensors) on the source's bearing that is caused by the lack of a third velocity component, which means each vector sensor's output power is not rotationally invariant. The contribution of the directional term is significant whenever the entries of  $K$  are on the order of those in  $J$ . This generally occurs when the array size is not too large; therefore, the greatest relative improvement in CRB due to the use of the extra velocity components occurs for small array sizes, low SNR's, or one-dimensional (1-D) geometries, as discussed in [3]. For example, a vector-sensor uniform linear array (ULA) on a rigid surface is able to determine both azimuth and elevation. Comparison of (25) and (24) shows that the entry of  $K$  corresponding to azimuth is larger relative to the corresponding entry of  $J$  than is the elevation entry of  $K$  relative to the elevation entry of  $J$ . Thus, in this scenario, adding the velocity sensors improves the ability to estimate azimuth more than it does elevation. This may again be attributed to the lack of a normal-component velocity signal on the rigid surface.

Fig. 2 shows  $\sqrt{\text{MSAE}_B}$  for the above two arrays with four sensors at the corners of a square with half-wavelength sides. This arrangement satisfies the condition of Section III, thereby making the bound a function of incidence angle alone. An SNR of 0 dB and 100 snapshots are assumed. Note that for all numerical examples, the SNR is defined as  $\sigma_s^2/\sigma^2$ , i.e., the SNR that would exist at a pressure sensor if the boundary were absent. The dotted curve is for the pressure-sensor array, and the solid is for the array of pressure sensors plus in-plane velocity components. The latter exhibits a 16% reduction in  $\sqrt{\text{MSAE}_B}$  for sources at normal (i.e.,  $0^\circ$ ) incidence, and the improvement steadily increases to 35% as the source approaches grazing incidence. Both arrays have poor optimal performance at large incidence angles because the CRB

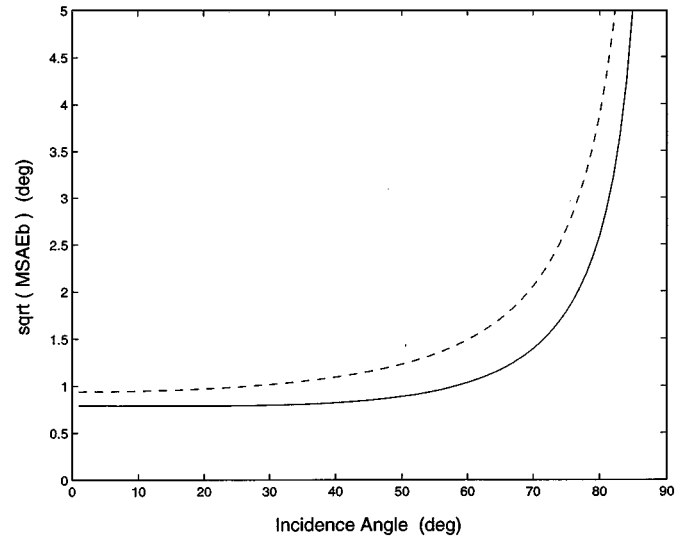


Fig. 2. Performance (in terms of  $\sqrt{\text{MSAE}_B}$ ) of pressure-sensor array on a rigid surface (dashed) and effect of adding in-plane velocity sensors at each location (solid).

on elevation (although not azimuth) tends to infinity as the incidence angle tends to  $90^\circ$  (see [3] for a discussion of what nonfiniteness of the CRB means in terms of the performance of actual estimators). Interestingly,  $\text{CRB}(\psi)$  would remain finite for a planar array of full (four-component) vector sensors in free space [3]. Therefore, the lack of an out-of-plane velocity signal makes a crucial difference to the finiteness of the bound. For a hull-mounted flank array, we expect that most signals of interest will come from within about  $60^\circ$  of normal incidence; at greater angles, the source is very nearly directly above or directly below the vessel and is better handled by an array on the top or bottom of the hull. Thus, the problems associated with large incidence angles do not really concern us in this scenario. From Fig. 2, we see that unlike the pressure-sensor curve, the vector-sensor curve is very flat over  $\gamma \in [0^\circ, 60^\circ]$ . Thus, we conclude that over the operational incidence angles of interest, adding the in-plane velocity components to a pressure-sensor array on a rigid surface improves the optimal performance (in this example by between 16% and 30%) and makes it more isotropic.

As shown in [3] an additional advantage of a vector-sensor array is that it does not suffer from ambiguities in an under-sampled wavefield. In the hull-mounted scenario, we may wish to use the same array over a wide range of frequencies. It may not be feasible or desirable to place the sensors so close that their separation is half a wavelength at the maximum end of the operating frequency. Indeed, this would lead to considerable degradation in performance at the lower end of the frequency band if this band spans many octaves. However, by using the in-plane velocity components, we can design our array with a separation corresponding to, say, the middle of the frequency band, yet not suffer from ambiguities at the upper end. As an example, Fig. 3 shows the 3-D normalized beam pattern of spatially undersampled vector-sensor and pressure-sensor arrays. The sensors are arranged on a regular  $3 \times 3$  grid with 1.5 wavelengths between adjacent sensors, and there is a single 0 dB source at an azimuth of  $45^\circ$  and an incidence angle of  $55.5^\circ$ . In the figure, the beam pattern is plotted against azimuth, and elevation is then

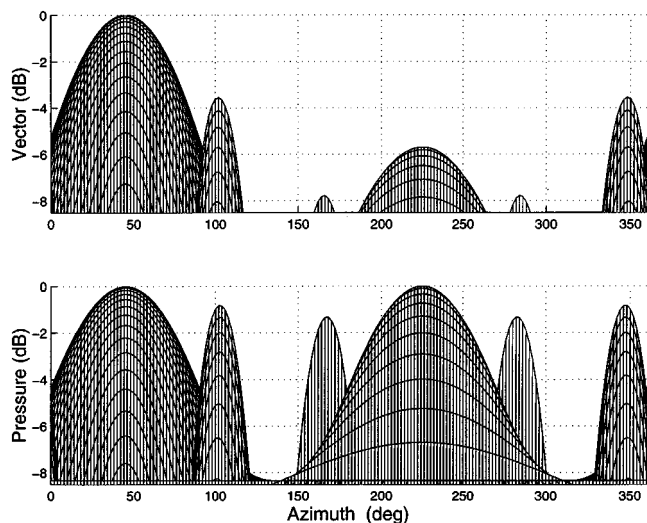


Fig. 3. Beampattern of  $3 \times 3$  regular spatially undersampled (1.5 wavelength spacing) pressure-sensor and vector-sensor arrays (pressure and in-plane velocity components only) on a rigid surface. There is a single 0 dB source at  $[45^\circ, 55.5^\circ]$ .

projected onto the azimuthal axis. It can be clearly seen that the pressure-sensor array's beampattern exhibits two indistinguishable global maxima leading to ambiguity, as well as several high secondary peaks, which can cause wide angle errors when only a finite number of samples are available. In the vector-sensor array's beampattern, however, the ambiguous grating lobe is reduced by about 6 dB relative to the mainlobe; the background level (not shown) is also 6 dB lower. Furthermore, the other secondary peaks are suppressed relative to the pressure-sensor plot, reducing the chances of wide angle errors. The amount by which they are reduced depends of their position relative to the mainlobe; in general, the further they are from the mainlobe, the greater the suppression. Naturally, since there is no normal velocity component, the array's ability to resolve ambiguities, i.e., to suppress grating lobes, is not as great as in the free-space scenario [3]. It is also clear that the achievable suppression, i.e., decibel reduction, may vary considerably with the locations of the source and grating lobes since  $|\mathbf{h}|^2 \rho$ , which may be thought of as the effective combined SNR at each sensor, varies with incidence angle. Again, this is in contrast to the free space situation.

Finally, by adding the in-plane velocity sensors, we can obtain a rapid wideband estimate of the azimuth, even with a single vector sensor, based on estimation of the horizontal component of acoustic intensity. In Section V-A, we develop such an estimator for an ocean bottom-mounted array; however, the development is equally applicable to the present case. Note, however, that unlike the seabed scenario considered in Section V-A, the lack of a normal velocity component on a rigid surface precludes development of a rapid wideband estimate of elevation. Nevertheless, the rapid azimuthal estimate would be very useful for reducing the search dimension to 1-D and/or providing initial estimates for a high-resolution estimator, such as maximum likelihood, that requires numerical optimization.

### B. Pressure-Release Boundary

The pressure-release boundary condition occurs whenever the surface is highly acoustically pliable, i.e., it offers no

resistance to motion when an acoustic wave hits it. In this case,  $\mathcal{R} = -1$  for all incidence angles; thus, from (3) and (4), we see that the pressure and in-plane velocity components are zero; this is the origin of the low signal problem encountered when using hull-mounted pressure sensors at low frequency. However, the normal velocity component is doubled at the surface, and thus, an array of normal-component velocity sensors can be mounted on the surface. To find the CRB, we use  $|\mathbf{h}|^2 = 4 \sin^2 \psi$  in the formulae of Section III, with  $K = 0$ . Therefore, in terms of CRB, the array is equivalent to a pressure-sensor array in free space with a directionally dependent SNR of  $4\rho \sin^2 \psi$ . As we might expect, the SNR tends to zero, and thus, the CRB goes to infinity, as the wave approaches grazing incidence, since the sensors then make no measurement. There is no geometry independent term  $K$ , in spite of the directional sensitivity of the velocity sensors, because there is no other component against which to reference the magnitude and phase of the normal velocity measurements. This emphasizes that the advantages of vector sensors for direction finding discussed in [3] are due to the use of sensing elements that measure diverse physical quantities rather than just the use of sensors with a directionally dependent response.

As discussed in Section II, the incident and reflected waves interfere to form a standing wave pattern. As we move away from the boundary, the pressure and in-plane velocities increase while the normal velocity decreases. In fact, from (12), we note that the pressure and in-plane velocities are proportional to  $1 - e^{-i\vartheta}$ , whereas the normal velocity is proportional to  $1 + e^{-i\vartheta}$ . Thus, the pressure and in-plane velocities are double their free-space values, and the normal velocity is zero when  $\vartheta = (2k - 1)\pi$  for any positive integer  $k$ . For a wave that is normally incident on the surface, this first occurs at a distance of a quarter wavelength from the boundary. For a wave of arbitrary incidence, this situation first occurs when  $d = 1/(4 \cos \gamma)$ , i.e., the greater the incidence angle, the further from the boundary pressure-doubling occurs. Clearly, one solution to the low pressure-signal problem is to mount an array of pressure sensors at a "stand-off" distance  $d$  from the boundary. However, the "stand-off" array solution is undesirable because it increases the vessel's profile and, hence, drag and sonar visibility. Furthermore, the longer the wavelength, the larger the stand-off distance required, and it is at low frequency that the pressure-release model is appropriate. Therefore, a question of considerable practical interest is to determine the minimum stand-off distance required of a pressure-sensor array in order for it to have comparable performance to a hull-mounted array of normal velocity sensors.

1) *Critical Distance:* To find the CRB for the stand-off array of pressure sensors, we set  $|\mathbf{h}|^2 = |1 - e^{-i\vartheta}|^2$  and  $K = 0$  in our derived expressions. Thus, its CRB is equivalent to a free-space pressure-sensor array with a directionally dependent SNR of  $4\rho \sin^2(\vartheta/2)$ . Comparing this with the CRB of an identical hull-mounted normal-component velocity sensor array, we see that they merely differ in their effective SNRs. In addition, since the CRBs of both arrays are monotonic decreasing functions of their SNRs, they have identical performance if and only if  $\sin^2(\vartheta/2) = \sin^2 \psi$ . We therefore define the critical stand-off distance as the smallest value of  $d$  for which the CRB's are

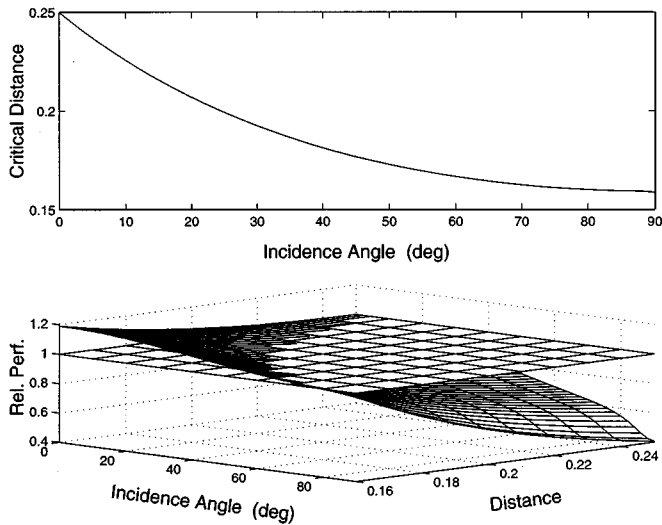


Fig. 4. Critical distance (in wavelengths) for a pressure release boundary at which a stand-off array of pressure sensors and a surface mounted array of normal-component velocity sensors have the same performance. The relative performance, i.e., ratio of  $\sqrt{\text{MSAE}_B}$  (pressure over velocity), for  $m\rho = 9$ , is also shown.

equal. It is a function of elevation alone given by

$$d_{\text{crit}} = \frac{\psi}{2\pi \sin \psi} \quad (26)$$

and is plotted (versus incidence angle  $\gamma = \pi/2 - \psi$ ) in the upper portion of Fig. 4. Note that the stand-off pressure-sensor array performs better in the region above the line and the surface-mounted velocity-sensor array in the region below. Remarkably,  $d_{\text{crit}}$  is completely independent of the array size, geometry, and signal and noise powers; therefore, this is a result of considerable generality. When  $d$  is a quarter wavelength, the stand-off array has a lower CRB for all incidence angles except zero (normal incidence), where they are equal. As the stand-off distance decreases, the hull-mounted array does better close to normal incidence and for  $d < 0.16$  wavelengths, it is better at all incidence angles. The performance of both arrays is poor when the incident wave is very far from normal (see Fig. 5), but as discussed in Section IV-A, the most useful range for a hull-mounted array is up to about  $60^\circ$  of incidence. As can be seen from Fig. 4, the hull-mounted array does better over most of this range if the pressure-sensor array's stand-off distance is reduced much below a quarter wavelength. For example, even with  $d = 0.2$  wavelengths (equivalent to 3 m at 100 Hz), the hull-mounted array is better for all incidence angles less than about  $25^\circ$ .

The lower plot in Fig. 4 shows the relative performance of the two arrays, which is defined as the ratio of the square root of the  $\text{MSAE}_B$  for the pressure-sensor array to that of the flush-mounted velocity sensor array, against both incidence angle and the stand-off distance of the pressure sensor array. The relative performance is actually (very mildly) dependent on  $m\rho$ , the product of the number of sensors and the SNR; the curve is shown for  $m\rho = 9$ . The velocity-sensor array has the lower  $\text{MSAE}_B$  and, hence, the better optimal performance when the curve is above the unit plane. The critical distance is the locus

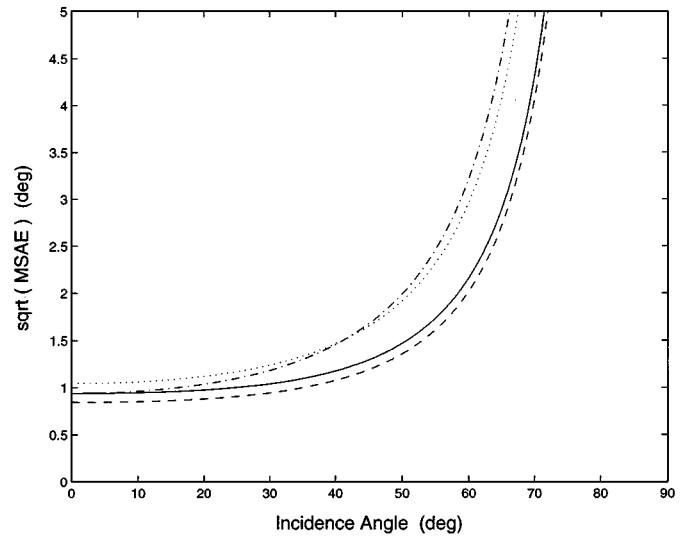


Fig. 5.  $\sqrt{\text{MSAE}_B}$  versus incidence angle for various four-element arrays at a pressure-release surface. The sensors lie a regular grid with half wavelength spacing; a 0-dB source and 100 snapshots are used. The solid line is the pressure array at  $d = 0.25$ , the dash-dotted line is a flush-mounted normal-component velocity array, the dotted line is a pressure array at  $d = 0.18$ , and the dashed line is a vector-sensor array at  $d = 0.14$ .

of the intersection of the surface with the unit plane and, as noted above, does not depend on  $m$  or  $\rho$ . The flush-mounted velocity-sensor array improves performance by up to 20% over a large range of incidence angles if the stand-off distance of the pressure-sensor array is reduced to much less than a quarter wavelength.

Fig. 5 gives a numerical comparison of the four-element square arrays with half wavelength spacing. The arrays have similar performance when the pressure-sensor array is at  $d = 0.18$  wavelengths; however, it becomes unacceptable for  $\gamma > 60^\circ$ . Therefore, in most of the useful region, the surface-mounted array is to be preferred. This confirms that if a stand-off distance of less than about 0.2 is required, the hull-mounted velocity sensor array provides a better solution. Fig. 5 also shows the performance of a full four-component vector-sensor array at a distance of  $d = 0.14$  wavelengths. It is similar to, but slightly better than, that of a pressure-sensor array at  $d = 0.25$ . Thus, by using vector sensors, we can outperform the hull-mounted array with a smaller stand-off distance.

### C. Layered-Hull Model

In this section, we use a realistic layered model for the hull. Here, all three components of acoustic particle velocity and the acoustic pressure are generally nonzero at the surface; therefore, we consider a flush-mounted array of full vector sensors and compare it with a similar array of pressure sensors. We model the hull as an air-backed steel plate with an absorptive, compliant coating or baffle. The coating, which is on the outside of the hull, serves the practical purpose of reducing noise levels at the sensors resulting from internal acoustic sources, rotating machinery, etc. The sensors themselves are flush-mounted on the exterior of the coating. References [29]–[31] discuss the design of velocity sensors for use on compliant baffles for hull-

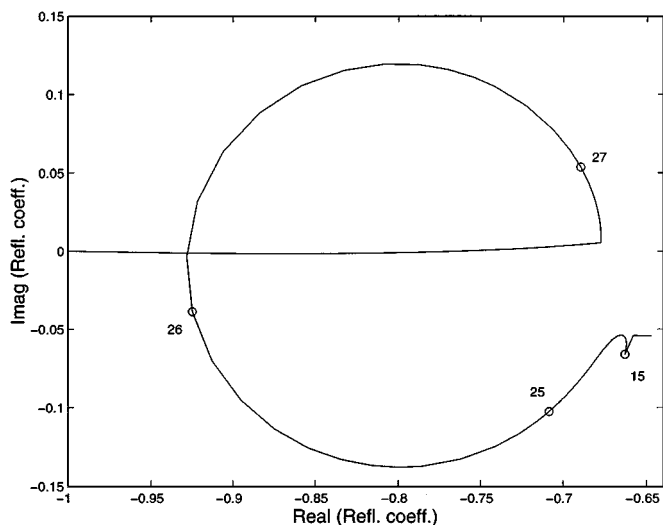


Fig. 6. Top: Real versus imaginary components of  $\mathcal{R}$  for layered hull at 1 kHz. Incidence angles (in degrees) of particular interest are indicated.

mounted arrays, and [32] presents experimental results using an array of velocity sensors mounted on such a steel backed coating at a U.S. Naval lake-test facility.

We use typical values for the hull and coating parameters as follows: The steel hull is taken to be 2 in thick, with density  $7900 \text{ Kg/m}^3$ , a longitudinal wave velocity of  $5710 \text{ m/s}$ , and shear wave velocity of  $3160 \text{ m/s}$ . We ignore absorption in the steel. The compliant coating has a thickness of 4 in and density  $\rho_c = 750 \text{ Kg/m}^3$ . It is assumed to have a Young's modulus of  $E_c = 1500(1 - 0.3i) \text{ psi}$ —the complex value accounts for absorption in the material—and Poisson's ratio  $\nu_c = 0.42$ . From these, the (complex) speeds of longitudinal and shear waves in the coating may be determined from

$$c_c = \sqrt{\frac{E_c(1 - \nu_c)}{\rho_c(1 + \nu_c)(1 - 2\nu_c)}} \quad (27)$$

$$b_c = \sqrt{\frac{E_c}{2\rho_c(1 + \nu_c)}} \quad (28)$$

respectively; see [33].

In order to calculate the CRB, we require the reflection coefficient and its derivative as functions of incidence angle. For this model, the expressions are very complex. We use the method of calculation presented in [20] to determine  $\mathcal{R}$  and extend this procedure to determine  $\partial\mathcal{R}/\partial\gamma$ , which is also needed in the calculations. The details are contained in [28]. The upper plot in Fig. 6 shows  $\mathcal{R}$  as it changes with incidence angle at 1 kHz. It has an absolute value of about 0.6 at normal incidence and tends to  $-1$  as the wave tends to grazing incidence. It changes very rapidly, and by quite a large amount, between  $25^\circ$  and  $27^\circ$ , reaching  $-0.9$  near  $26^\circ$  of incidence. This is due to the fact that the shear wave in the steel reaches its point of total internal reflection and becomes a surface wave in this region. A much smaller rapid change in  $\mathcal{R}$  also occurs around  $15^\circ$  when the longitudinal wave in the steel becomes a surface wave, but it is barely perceptible. Note that  $\mathcal{R}$  has a fairly small imaginary part relative to its real part. In the present scenario,  $\mathcal{R}$  is also dependent on frequency;

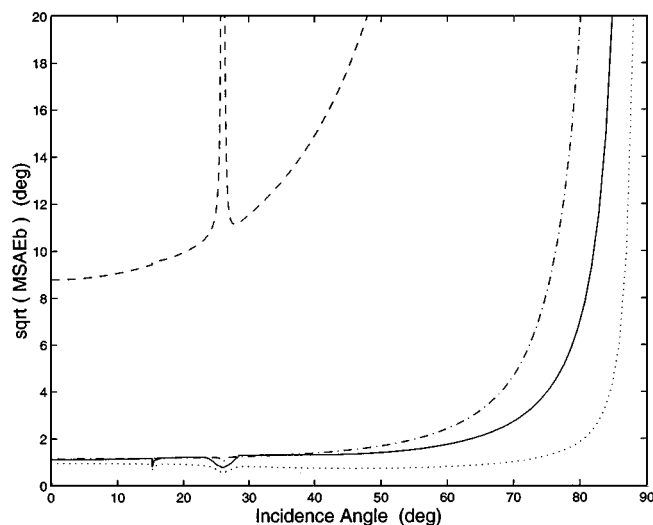


Fig. 7.  $\sqrt{\text{MSAE}_B}$  versus incidence angle for various four-element arrays at layered hull. The sensors lie a regular grid with half wavelength spacing; a 0-dB, 1-kHz source and 100 snapshots are used. The solid and dashed lines are flush-mounted vector-sensor and pressure-sensor arrays, respectively. The dotted and dash-dotted lines are vector-sensor and pressure-sensor arrays at  $d = 0.25$ .

however, at all frequencies we investigated,  $\mathcal{R}$  starts somewhere in the left half of the plane and tends to  $-1$  as the wave tends to grazing.

Fig. 7 compares  $\sqrt{\text{MSAE}_B}$  for flush-mounted and stand-off vector-sensor and pressure-sensor arrays. The array shape is again four sensors at the corners of a square with half-wavelength sides, and  $\mathcal{R}$  is calculated at 1 kHz. The flush-mounted pressure-sensor array (FPA) performs very poorly because all incidence angles  $\mathcal{R} + 1$  and, hence, the pressure signal at the boundary are quite small. The performance is particularly poor around  $\gamma = 26^\circ$  and near grazing incidence because  $\mathcal{R}$  approaches  $-1$  in these regions, and thus, the surface almost becomes pressure release. The others arrays exhibit no dramatic drop in performance (and even a slight improvement) at  $\gamma = 26^\circ$  for the following reasons.

- i) Flush-mounted vector-sensor array (FVA): The increase in normal component signal outweighs the drop in pressure and in-plane velocity signals, which are relatively small anyway.
- ii) Stand-off pressure-sensor array (SPA): The pressure signal becomes quite large.
- iii) Stand-off vector-sensor array (SVA): The pressure and in-plane signals become bigger and outweigh the drop in normal velocity signal, which is relatively small anyway.

The small but abrupt change in  $\mathcal{R}$  around  $\gamma = 15^\circ$  causes a 20% improvement in both vector-sensor array bounds (just visible) but has very little effect on the pressure-sensor arrays. The SPA has about the same performance as the FVA, except for larger incidence angles, where it does worse. Thus, by using vector sensors, a flush-mounted deployment can be used with no loss in performance. The SVA, however, does improve somewhat on the FVA, particularly at large incidence, but the increase in performance is probably outweighed by the need to keep the vessel's profile to a minimum. Note that the stand-off distance of 0.25 wavelengths corresponds to 0.75 m at 1 kHz.

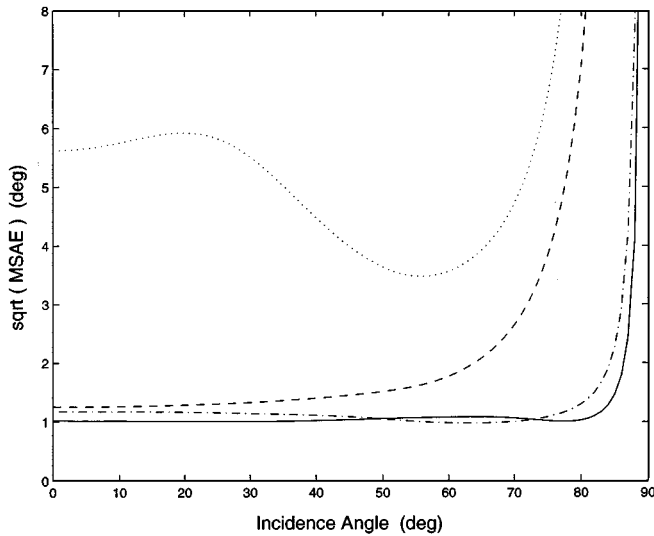


Fig. 8.  $\sqrt{\text{MSAE}_B}$  versus incidence angle for various four-element arrays near the seabed arranged as a regular grid with half wavelength spacing with a 0-dB source and 100 snapshots. The absorption coefficient  $\alpha = 0.1$ . The solid and dashed lines are vector-sensor and pressure-sensor arrays, respectively, at the surface. The dash-dotted and dotted lines are the same arrays at  $d = 0.25$ .

## V. SEABED

Passive listening arrays mounted on the seabed have important military and civilian applications [34]. There are numerous ways in which sensors can be bottom mounted: in ballasted trawl-resistant casings dropped from the surface, tethered to a frame, positioned by a diver or underwater vehicle, etc. [35]. Depending on which design is chosen, it is possible to have the sensors lying essentially at the boundary or at some known distance above it.

The interface between sea water and the packed sandy ocean bottom can be approximately modeled as the boundary between two fluids, one of which is absorptive [20], [36]. The reflection coefficient is given by

$$\mathcal{R}(\gamma) = \frac{\eta \cos \gamma - i(\sin^2 \gamma - n^2)^{1/2}}{\eta \cos \gamma + i(\sin^2 \gamma - n^2)^{1/2}} \quad (29)$$

where  $\eta$  is the ratio of sand density to water density, and  $n$  is the index of refraction. The presence of absorption is accounted for by assuming that the index of refraction is complex, i.e.,  $n = n_0(1 + i\alpha)$ , with  $\alpha > 0$ . We use the typical values  $n_0 = 0.83$ ,  $\eta = 2.7$ ,  $\alpha = 0.1$  [20, p. 11]. Fig. 8 compares vector-sensor and pressure-sensor arrays mounted at or near the seabed. It can be seen that the vector-sensor array performs better than the pressure-sensor array and has a virtually isotropic performance over almost the whole range of incidence angles. The improvement in performance is particularly noticeable when the array is mounted a quarter wavelength from the boundary when the pressure-sensor array's performance is considerably poorer and highly dependent on the incidence angle.

### A. Fast Wideband Estimator

We now present a fast wideband localization algorithm for use with a single vector sensor located on the seabed. Acoustic intensity is a vector quantity defined as the product of pressure and velocity. Since the  $x$  and  $y$  components of the wavenumber

vector of an incident wave are unaltered on reflection, the horizontal component of the acoustic intensity vector is parallel to the projection of the incident (and reflected) wavenumber vector. Furthermore, since the incident wavenumber vector defines the direction to the source, we can use an estimate of the horizontal acoustic intensity to determine the azimuth. Note that [2] used this technique to derive an estimator for the full bearing vector using a vector sensor in free space; however, it cannot be used to find the elevation when the boundary is present.

The horizontal component of acoustic intensity measured by a single vector sensor located a distance  $d$  from a reflecting boundary is

$$\mathbf{I}_h(t) = y_p(t)[y_{v_x}(t), y_{v_y}(t)]^H. \quad (30)$$

Thus, as long as the noise at the various sensors is mutually uncorrelated

$$\mathbb{E}\{\mathbf{I}_h(t)\} = \sigma_s^2 |1 + \mathcal{R}e^{-i\vartheta}|^2 \cos \psi \begin{bmatrix} \cos \hat{\phi} \\ \sin \hat{\phi} \end{bmatrix}. \quad (31)$$

Since this is purely real, we let  $\hat{\mathbf{s}} = N^{-1} \sum_{t=1}^N \text{Re}\{\mathbf{I}_h(t)\}$ , and by the strong law of large numbers,  $\hat{\mathbf{s}} \rightarrow \mathbb{E}\{\mathbf{I}_h(t)\}$ . Thus, we can estimate azimuth from

$$\begin{bmatrix} \cos \hat{\phi} \\ \sin \hat{\phi} \end{bmatrix} \triangleq \frac{\hat{\mathbf{s}}}{\|\hat{\mathbf{s}}\|} \rightarrow \begin{bmatrix} \cos \phi \\ \sin \phi \end{bmatrix}. \quad (32)$$

With appropriate modification, we can apply the analysis of [2, App. B] to this azimuthal estimator to show that its asymptotic MSAE is

$$\lim_{N \rightarrow \infty} NE(\hat{\phi} - \phi)^2 = \frac{1 + |1 + \mathcal{R}|^2 \rho}{2\rho^2 |1 + \mathcal{R}|^4 \cos^2 \psi} \quad (33)$$

where  $\rho = \sigma_s^2 / \sigma^2$  is the SNR. Note that this estimator does not require a normal velocity sensor or knowledge of the reflection properties of the boundary (or even the distance to the boundary).

In contrast, to obtain an estimate of the elevation, we require a normal velocity sensor, and we need to know the reflection characteristics of (and distance to) the ocean bottom. The vertical component of acoustic intensity  $I_v(t) \triangleq y_p(t)y_{v_z}^H(t)$  has expected value

$$\mathbb{E}\{I_v(t)\} = \sigma_s^2 (1 + \mathcal{R}e^{-i\vartheta})(1 - \mathcal{R}^H e^{i\vartheta}) \sin \psi. \quad (34)$$

Using (31), we note that

$$\frac{\mathbb{E}\{I_v(t)\}}{\|\mathbb{E}\{\mathbf{I}_h(t)\}\|} = \frac{1 - \mathcal{R}^H e^{i\vartheta}}{1 + \mathcal{R}^H e^{i\vartheta}} \tan \psi \triangleq \chi. \quad (35)$$

The quantity on the right-hand side,  $\chi$  say, is a function of  $\psi$  alone, which we estimate from the statistic

$$\hat{\chi} = \frac{\sum_{t=1}^N I_v(t)}{\left\| \sum_{t=1}^N \text{Re}\{\mathbf{I}_h(t)\} \right\|}. \quad (36)$$

It then remains to solve

$$\hat{\chi} = \frac{1 - \mathcal{R}(\hat{\psi})^H e^{i4\pi d \sin \hat{\psi}}}{1 + \mathcal{R}(\hat{\psi})^H e^{i4\pi d \sin \hat{\psi}}} \tan \hat{\psi} \quad (37)$$

for  $\hat{\psi}$ .

In general, (37) must be solved using a 1-D numerical search. However, if the sensor lies at the interface, i.e.,  $d = 0$ , the right-hand side of (37) becomes  $\rho_0 c / Z_{\text{in}}^H(\hat{\psi}) \cos \hat{\psi}$ . For the seabed scenario, we can then solve (37) analytically. Using (29), we have

$$\frac{1 - \mathcal{R}^H}{1 + \mathcal{R}^H} \tan \psi = \frac{-i \sqrt{\cos^2 \psi - n^2}}{\eta \cos \psi} \quad (38)$$

and hence, we obtain a rapid wideband estimate for the elevation using

$$\hat{\psi} = \text{Re} \left\{ \cos^{-1} \left| \frac{n}{\sqrt{\hat{\chi}^2 \eta^2 + 1}} \right| \right\}. \quad (39)$$

The real value of the inverse cosine is taken to deal with (rare) cases in which the argument is larger than one, in which case,  $\hat{\psi} = 0$ . We determined by numerical simulation that taking absolute values before the inverse cosine gave slightly greater accuracy than taking real values or applying the inverse cosine to a complex number, particularly for large  $N$ . Note that the bandwidth is limited only by the frequency range over which the input impedance  $Z_{\text{in}}$ , or equivalently  $\mathcal{R}$ , is approximately constant. Since  $\mathcal{R}$  is independent of frequency in (29), it is restricted only by the range of frequencies over which the fluid-fluid model is valid for reflection from the seabed.

Fig. 9 shows the performance of this estimator as a function of incidence angle. From Fig. 9, we see that our estimator is not far from the optimal bound over quite a large range of source locations and approaches it at normal incidence ( $0^\circ$ ). After about  $55^\circ$ , however, the estimator's performance falls off very rapidly, whereas the bound actually becomes smaller. This is mainly due to rapid deterioration of the elevation estimate, as indicated by the fact that its empirical standard deviation closely tracks the empirical MSAE. Further investigations reveal that  $\hat{\chi}$  is a very good estimator of  $\chi$  below  $55^\circ$  but becomes highly biased at larger incidence angles. Increasing the number of snapshots does not seem to solve the problem; therefore,  $\hat{\chi}$  appears to be an inconsistent estimate of  $\chi$  at large incidence angles, thereby resulting in the poor performance. Despite this, the estimator is very effective over a large range of input angles and would certainly be very effective at, for example, locating surface vessels since the incidence angle is very unlikely to be more than  $55^\circ$ . Note that because of the symmetry of the problem, the performance is independent of azimuth.

## VI. CONCLUSION

We have developed a general model for the measurements made by a vector-sensor array located at or near an arbitrary plane reflecting boundary and derived an expression for the

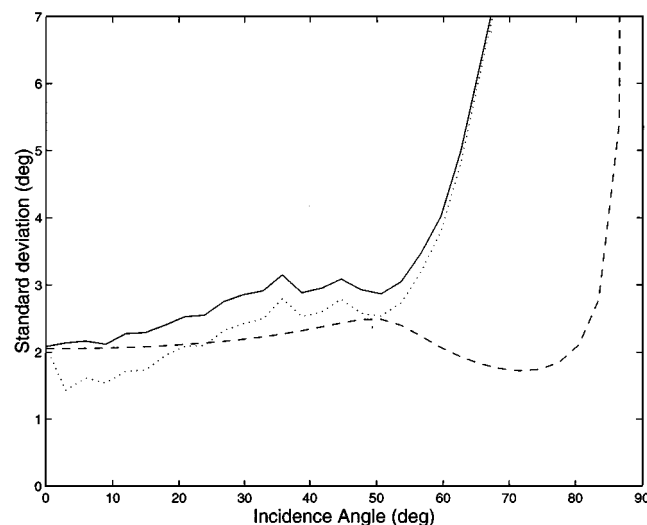


Fig. 9. Comparison of empirical  $\sqrt{\text{MSAE}}$  of the fast wideband estimator (solid) with the bound  $\sqrt{\text{MSAE}_B}$  (dashed) for a 3-dB source with 200 snapshots and absorption coefficient  $\alpha = 0.1$ . The empirical standard error of the elevation estimate (dotted) is also shown. For each incidence angle, 500 realizations were used.

Cramér-Rao bound and, hence, a bound on mean-square angular error of a single source. The hull-mounted and seabed applications were considered in detail. For the hull-mounted application, the special cases of rigid (high-frequency) and pressure-release (low-frequency) boundaries were studied in detail, as well as a more complex, realistic layered model for the hull. At the rigid surface, the use of in-plane and velocity components improved performance over a pressure-sensor array, particularly for angles far from incidence. Using the beam patterns, we also showed that the addition of the in-plane components resolved ambiguities caused by spatial undersampling. For the pressure-release surface, we showed that normal-component velocity sensors could be used to overcome the low-pressure signal problem at such a surface; this was a matter of considerable practical interest in low-frequency hull-mounted sonar. In this case, a comparison was made between a surface-mounted array of velocity sensors and a stand-off array of pressure-sensors. The critical distance at which the arrays have the same performance was introduced, and a simple expression depending solely on the incidence angle was derived. Although the pressure-sensor array performed better at a quarter wavelength, the surface-mounted array was to be favored if the stand-off distance dropped much below 0.2 wavelengths. Furthermore, the use of vector sensors allowed a much smaller stand-off distance than 0.25 while maintaining the performance advantage. By using the realistic layered model, we showed that, generally, using a flush-mounted array of full four-component vector sensors, it is possible to outperform a stand-off pressure sensor array at any stand-off distance.

For the seabed application, we modeled the ocean floor using an absorptive liquid layer. We quantified the potential improvement of using vector sensors over traditional pressure sensors when mounted directly on the bottom and when mounted slightly above, as in a moored deployment. We showed that the vector-sensor array fared considerably better, particularly in the moored deployment, and had an almost isotropic performance.

For this scenario, we also derived and analyzed a fast wideband estimator for use with an even single vector sensor.

Future work for the hull-mounted scenario could incorporate the problems associated with nonacoustic vibrations of the surface, e.g., from machinery noise, as well as consider curved boundaries. For the seabed, more complex models of the bottom and near-field sources could be incorporated, as well as propagation models in littoral regions.

## REFERENCES

- [1] A. Nehorai and E. Paldi, "Acoustic vector-sensor array processing," in *Proc. 26th Asilomar Conf. Signals, Syst., Comput.*, Pacific Grove, CA, 1992, pp. 192–198.
- [2] —, "Acoustic vector-sensor array processing," *IEEE Trans. Signal Processing*, vol. 42, pp. 2481–2491, Sept. 1994.
- [3] M. Hawkes and A. Nehorai, "Acoustic vector-sensor beamforming and Capon direction estimation," *IEEE Trans. Signal Processing*, vol. 46, pp. 2291–2304, Sept. 1998.
- [4] —, "Effects of sensor placement on acoustic vector-sensor array performance," *IEEE J. Oceanic Eng.*, vol. 24, pp. 33–40, Jan. 1999.
- [5] M. J. Berliner and J. F. Lindberg, *Acoustic Particle Velocity Sensors: Design, Performance and Applications*, M. J. Berliner and J. F. Lindberg, Eds. Woodbury, NY: AIP, 1996.
- [6] K. T. Wong and M. D. Zoltowski, "Self-initiating beamspace MUSIC for underwater acoustic direction-finding with irregularly spaced vector-hydrophones," in *Proc. IEEE Int. Symp. Circ. Syst.*, Hong Kong, June 1997, pp. 2553–2556.
- [7] —, "Closed-form underwater acoustic direction-finding with arbitrarily spaced vector hydrophones at unknown locations," *IEEE J. Oceanic Eng.*, vol. 22, pp. 566–575, July 1997.
- [8] —, "Extended-aperture underwater acoustic multisource azimuth/elevation direction-finding using uniformly but sparsely-spaced vector hydrophones," *IEEE J. Oceanic Eng.*, vol. 22, pp. 659–672, Oct. 1997.
- [9] —, "Root-MUSIC-based azimuth-elevation angle-of-arrival estimation with uniformly spaced but arbitrarily oriented velocity hydrophones," *IEEE Trans. Signal Processing*, vol. 47, pp. 3250–3260, Dec. 1999.
- [10] J. C. Nickles *et al.*, "A vertical array of directional acoustic sensors," in *Proc. Mast. Oceans Tech.*, Newport, RI, Oct. 1992, pp. 340–345.
- [11] G. L. D'Spain *et al.*, "Initial analysis of the data from the vertical DIFAR array," in *Proc. Mast. Oceans Tech.*, Newport, RI, Oct. 1992, pp. 346–351.
- [12] M. Hawkes and A. Nehorai, "Battlefield target localization using acoustic vector sensors and distributed processing," in *Proc. Meet. IRIS Specialty Group Battlefield Acoust. Seismics*, Laurel, MD, Sept. 1999, pp. 111–128.
- [13] —, "Distributed processing for 3-D localization using acoustic vector sensors on the seabed or battlefield," in *Proc. 8th Ann. Adapt. Sensor Array Process. Workshop*, Lexington, MA, Mar. 2000.
- [14] —, "Hull-mounted acoustic vector-sensor array processing," in *Proc. 29th Asilomar Conf. Signals, Syst., Comput.*, Pacific Grove, CA, Oct. 1995, pp. 1046–1050.
- [15] —, "Surface-mounted acoustic vector-sensor array processing," in *Proc. Int. Conf. Acoust., Speech, Signal Processing*, GA, May 1996, pp. 3170–3173.
- [16] A. Nehorai and M. Hawkes, "Performance bounds for estimating vector systems," *IEEE Trans. Signal Processing*, vol. 48, pp. 1737–1749, June 2000.
- [17] A. Nehorai and E. Paldi, "Vector-sensor array processing for electromagnetic source localization," *IEEE Trans. Signal Processing*, vol. 42, pp. 376–398, Feb. 1994.
- [18] S. H. Ho, "Performance of velocity sensor for flexural wave reduction," in *Acoustic Particle Velocity Sensors: Design, Performance and Applications*, M. J. Berliner and J. F. Lindberg, Eds. Woodbury, NY: AIP, 1996, pp. 374–389.
- [19] S. H. Ho and H. H. Schloemer, "Signal pressure received by a hydrophone placed on a plate backed by a compliant baffle," *J. Acoust. Soc. Amer.*, vol. 89, pp. 559–564, 1991.
- [20] L. M. Brekhovskikh, *Waves in Layered Media*, 2nd ed. New York: Academic, 1980.
- [21] A. D. Pierce, *Acoustics—An Introduction to its Physical Principles and Applications*. New York: McGraw-Hill, 1981.
- [22] K. F. Sander and G. A. L. Reed, *Transmission and Propagation of Electromagnetic Waves*, 2nd ed. Cambridge, U.K.: Cambridge Univ. Press, 1986.
- [23] T. F. W. Embleton, J. E. Piercy, and N. Olson, "Outdoor sound propagation over ground of finite impedance," *J. Acoust. Soc. Amer.*, vol. 59, pp. 267–277, 1976.
- [24] M. Hawkes and A. Nehorai, "Pressure and velocity correlations in ambient noise," *IEEE J. Oceanic Eng.*, to be published.
- [25] G. C. Lauchle, J. F. McEachern, A. R. Jones, and J. A. McConnell, "Flow-induced noise on pressure gradient hydrophones," in *Acoustic Particle Velocity Sensors: Design, Performance and Applications*, M. J. Berliner and J. F. Lindberg, Eds. Woodbury, NY: AIP, 1996, pp. 202–225.
- [26] S. H. Ko and H. H. Schloemer, "Flow noise reduction techniques for a planar array of hydrophones," *J. Acoust. Soc. Amer.*, vol. 92, pp. 3409–3424, 1992.
- [27] T. S. Ferguson, *A Course in Large Sample Theory*. London, U.K.: Chapman & Hall, 1996.
- [28] M. Hawkes and A. Nehorai, "Acoustic vector-sensor processing in the presence of a reflecting boundary," Dept. Elect. Eng. Comp. Sci., Univ. Illinois, Chicago, Tech. Rep. UIC-EECS-99-8, Dec. 1999.
- [29] J. J. Caspall, G. W. Caille, J. Jarzynski, and G. S. McCall, III, "(3,1) PVDF acoustic displacement sensor," in *Acoustic Particle Velocity Sensors: Design, Performance and Applications*, M. J. Berliner and J. F. Lindberg, Eds. Woodbury, NY: AIP, 1996, pp. 134–143.
- [30] M. B. Moffett and J. M. Powers, "A bimorph flexural-disk accelerometer for underwater use," in *Acoustic Particle Velocity Sensors: Design, Performance and Applications*, M. J. Berliner and J. F. Lindberg, Eds. Woodbury, NY: AIP, 1996, pp. 69–83.
- [31] S. T. Vohra, B. Danver, A. Tveten, and A. Dandridge, "Fiber optic interferometric accelerometers," in *Acoustic Particle Velocity Sensors: Design, Performance and Applications*, M. J. Berliner and J. F. Lindberg, Eds. Woodbury, NY: AIP, 1996, pp. 285–293.
- [32] B. A. Cray and R. A. Christman, "Acoustic and vibration performance evaluations of a velocity sensing hull array," in *Acoustic Particle Velocity Sensors: Design, Performance and Applications*, M. J. Berliner and J. F. Lindberg, Eds. Woodbury, NY: AIP, 1996, pp. 177–178.
- [33] S. P. Timoshenko and J. N. Goodier, *Theory of Elasticity*, 3rd ed. New York: McGraw-Hill, 1970.
- [34] C. W. Clark, M. L. Tasker, M. Ferguson, J. P. Hartley, I. Fletcher, A. Whitehead, A. A. Duff, J. F. Appelbee, C. Pickton, J. Spink, C. MacDuff-Duncan, S. J. Knight, A. H. Walls, A. Onder, J. Urbanus, and I. Buchanan, "Monitoring the occurrence of large whales off north and west Scotland using passive acoustic arrays," in *Proc. SPE/UKOOA Euro. Environ. Conf.*, Aberdeen, U.K., Apr. 1997, pp. 23–29.
- [35] S. Kery and J. D. Irish, "Trawl resistant bottom mounted instrumentation: Developments and results to date," in *Proc. MTS/IEEE Oceans Conf.*, Fort Lauderdale, FL, Sept. 1996, pp. 640–645.
- [36] L. Jing-Fang and M. Hodgson, "Development and evaluation of equivalent-fluid approximations for sea-bottom sound reflection," *Canad. Acoust.*, vol. 26, pp. 3–11, Mar. 1998.



**Malcolm Hawkes** (S'95–M'00) was born in Stockton-on-Tees, U.K. in 1970 and grew up in Swansea, U.K. He received the B.A. degree in electrical and information science from the University of Cambridge, Cambridge, U.K., in 1992, the M.Sc. degree in applied statistics from the University of Oxford, Oxford, U.K., in 1993, and the M.S. and M.Phil. degrees in electrical engineering from Yale University, New Haven, CT, in 1995 and 1998, respectively. He will receive the Ph.D. degree in electrical engineering from Yale University, New Haven, CT, in December 2000.

From 1988 to 1989, and again in the summers of 1990 and 1991, he was with GEC-Marconi Research Centre, Chelmsford, U.K., on a variety of projects. Since 1996, he has been a Visiting Scholar at the University of Illinois, Chicago. His research interests include statistical signal processing with applications in array processing, communications, and biomedicine.

Mr. Hawkes received the John and Grace Nuveen International Scholar Award from the University of Illinois, Chicago, in 1998.



**Arye Nehorai** (S'80–M'83–SM'90–F'94) received the B.Sc. and M.Sc. degrees in electrical engineering from the Technion—Israel Institute of Technology, Haifa, in 1976 and 1979, respectively, and the Ph.D. degree in electrical engineering from Stanford University, Stanford, CA, in 1983.

After graduation, he worked as a Research Engineer for Systems Control Technology, Inc., Palo Alto, CA. From 1985 to 1995, he was with the Department of Electrical Engineering, Yale University, New Haven, CT, where he became an Associate Professor in 1989. In 1995, he joined the Department of Electrical Engineering and Computer Science, University of Illinois, Chicago (UIC), as a Full Professor. He is currently Chair of the Department's Electrical and Computer Engineering Division. He holds a joint professorship with the Bioengineering Department at UIC. His research interests are in signal processing, communications, and biomedicine.

Dr. Nehorai is Editor-in-Chief of the IEEE TRANSACTIONS ON SIGNAL PROCESSING and an Associate Editor of *Circuits, Systems, and Signal Processing* and *The Journal of the Franklin Institute*. He is also a Member of the Editorial Board of *Signal Processing*. He has previously been an Associate Editor of the IEEE TRANSACTIONS ON ACOUSTICS, SPEECH AND SIGNAL PROCESSING, IEEE SIGNAL PROCESSING LETTERS, the IEEE TRANSACTIONS ON ANTENNAS AND PROPAGATION, and the IEEE JOURNAL OF OCEANIC ENGINEERING. He served as Chairman of the Connecticut IEEE Signal Processing Chapter from 1986 to 1995 and is a Founding Member, and current Chair, of the IEEE Signal Processing Society's Technical Committee on Sensor Array and Multichannel (SAM) Processing. He was the co-General Chair of the First IEEE SAM Signal Processing Workshop in March 2000. He was co-recipient, with P. Stoica, of the 1989 IEEE Signal Processing Society's Senior Award for Best Paper. He has been a Fellow of the Royal Statistical Society since 1996.